PALEOCEANOGRAPHY, VOL. 28, 1–13, doi:10.1029/2012PA002326, 2013

A near-field sea level record of East Antarctic Ice Sheet instability from 32 to 27 Myr

Stephen J. Gallagher,[1] Giuliana Villa,[2] Russell N. Drysdale,[3] Bridget S. Wade,[4] Howie Scher,[5] Qianyu Li,[6] Malcolm W. Wallace,[1] and Guy R. Holdgate[1]

Received 27 March 2012; revised 29 October 2012; accepted 6 November 2012

[1] Fossil, facies, and isotope analyses of an early high-paleolatitude (55°S) section suggests a highly unstable East Antarctic Ice Sheet from 32 to 27 Myr. The waxing and waning of this ice sheet from 140% to 40% of its present volume caused sea level changes of ±25 m (ranging from -30 to +50 m) related to periodic glacial (100,000 to 200,000 years) and shorter interglacial events. The near-field Gippsland sea level (GSL) curve shares many similarities to the far-field New Jersey sea level (NJSL) estimates. However, there are possible resolution errors due to biochronology, taphonomy, and paleodepth estimates and the relative lack of lowstand deposits (in NJSL) that prevent detailed correlations with GSL. Nevertheless, the lateral variations in sea level between the GSL section and NJSL record that suggest ocean siphoning and antisiphoning may have propagated synchronous yet variable sea levels.

Citation: Gallagher, S. J., G. Villa, R. N. Drysdale, B. S. Wade, H. Scher, Q. Li, M. W. Wallace, and G. R. Holdgate (2013), A near-field sea level record of East Antarctic Ice Sheet instability from 32 to 27 Myr, *Paleoceanography*, *28*, doi: 10.1029/2012PA002326.

1. Introduction

[2] The early Cenozoic Earth was dominated by greenhouse conditions without permanent ice caps. Declining CO_2 in the atmosphere [*Pearson et al*., 2009] and cooling in the Eocene culminated in East Antarctic Ice Sheet expansion by the early Oligocene and the onset of icehouse conditions [*Zachos et al*., 2001] (Oi-1 around 33.7 Ma; see the time scale of *Gradstein et al*. [2004]). CO_2 estimates for the period from 32 to 27 Myr fluctuate from ~400 to ~600 ppmv [*Beerling and Royer*, 2011; *Pagani et al*., 2005], within the range of modern concentrations and those projected by the year 2100 [*Solomon*, 2007]. Knowledge of the early history of the East Antarctic Ice Sheet during these "modern-analogue" conditions is important if we are to project its future behavior under conditions of enhanced greenhouse warming. Records of early Oligocene glacioeustatic events are rare and based on the interpretation of oxygen ($\delta^{18}O$) isotope excursions in deep-sea sections such as Ocean Drilling Program (ODP) Site 1218 [*Pälike et al*., 2006; *Wade and Pälike*, 2004], ASP-5 [*Katz et al*., 2011], and Northern Hemisphere sequence stratigraphy records like the New Jersey (NJ) margin in the United States [*Pekar and Christie-Blick*, 2008; *Pekar et al*., 2001, 2002, 2006]. In the Southern Hemisphere, early Oligocene records of glacioeustatic events are rare and confined mainly to poorly sampled subsurface sections or attenuated subcrop/outcrop in Antarctica [*Barrett*, 1989]. Here we present for the first time the results of a detailed microfossil (foraminiferal/nannofossil), $\delta^{18}O$ isotope, and facies analyses of a subsurface cored section (Groper-1, hereinafter referred to as G-1) of Oligocene age from the offshore Gippsland Basin, southeast Australia. During this time the region lay at around 55°S [*Stickley et al*., 2004] (Figure 1) facing the evolving Tasman Sea. The results show a 5 million year (32–27 Ma) record of variable sea level indicating a highly unstable early Antarctic ice sheet. The waxing and waning of this ice sheet from 140% to 40% of its present volume caused sea level changes from -30 to +50 m relative to present.

2. Study Area, Materials, and Methods

[3] Our investigation involved the collection of detailed microfossil, stable isotope, and facies of a near-continuous core from Groper-1 petroleum exploration well (drilled in 1968 by ESSO Australia, Ltd., latitude 38° 56′ 30′S, longitude 147° 24′ 56′E) in the Gippsland Basin off southeast Australia (Figure 1). Eighty meters of core were drilled in this section with 80% recovery. Seventy-eight meters of core (Figure 2) were logged and sampled for facies, microfossil, and stable isotope ($\delta^{13}C$/ $\delta^{18}O$) analyses. Detailed wireline log data were used to enhance the facies analyses

All Supporting Information may be found in the online version of this article.

[1]School of Earth Sciences, University of Melbourne, Melbourne, Victoria, Australia.
[2]Dipartimento di Scienze della Terra, Università di Parma, Parma, Italy.
[3]Department of Resource Management and Geography, University of Melbourne, Melbourne, Victoria, Australia.
[4]School of Earth and Environment, University of Leeds, Leeds, UK.
[5]Department of Earth and Ocean Sciences, University of South Carolina, Columbia, South Carolina, USA.
[6]School of Ocean and Earth Sciences, Tongji University, Shanghai, China.

Corresponding author: S. J. Gallagher, School of Earth Sciences, University of Melbourne, Melbourne, VIC 3010, Australia. (sjgall@unimelb.edu.au)

0883-8305/13/2012PA002326

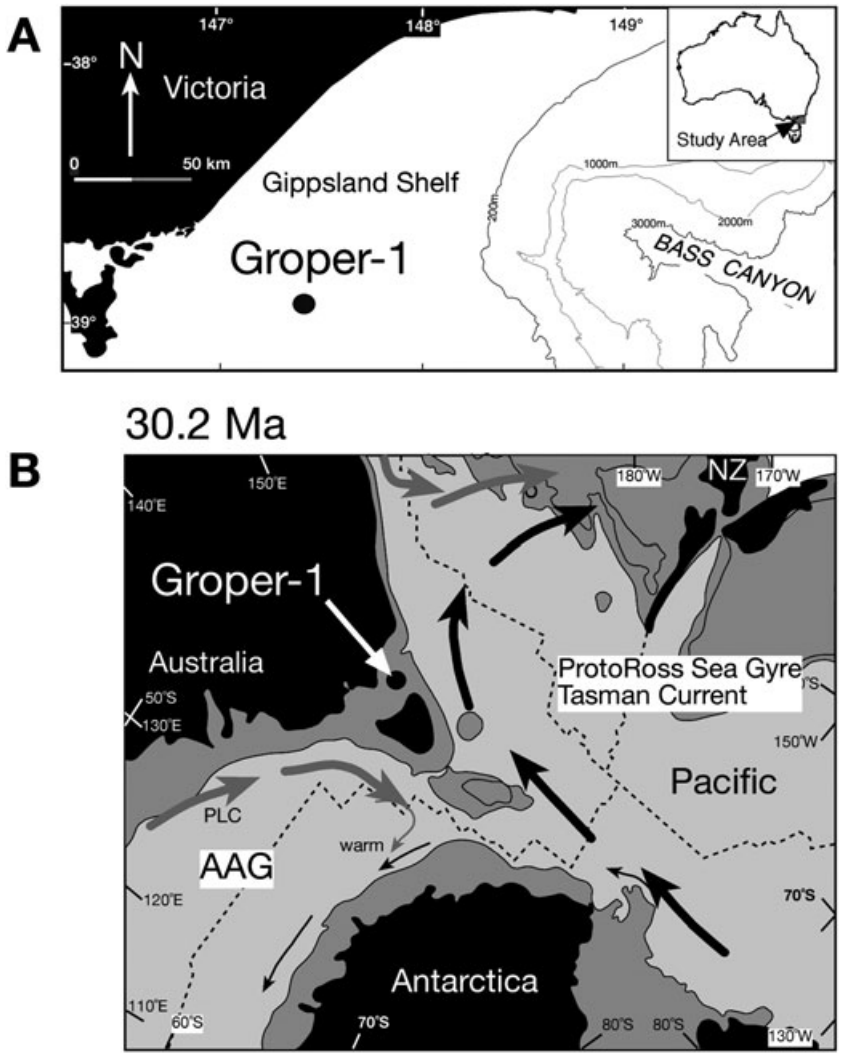

Figure 1. (a) The location of the Groper-1 cored section and (b) its Oligocene paleogeographic position at 30.2 Ma [*Stickley et al*., 2004]. Black arrows, cool currents; gray arrows, warm currents. AAG, Australo-Antarctic Gulf.

and to interpret intervals where there are core gaps. Fifteen thin sections of cemented horizons were analyzed for their microfacies. Carbonate content analyses using the volumetric technique of *Wallace et al*. [2002] were carried out on 190 samples (Figure 2). The carbonate facies were classified based on carbonate content and grain size using the limestone/marl/clay classification by *Pettijohn* [1975].

[4] Fifty-two samples were processed for presence/absence nannofossil biostratigraphy. Nannofossil preparation followed the standard technique of smear slides; analyses were performed with a light microscope ×1200 magnification. The nannofossil zonations of *Martini* [1971] and *Okada and Bukry* [1980] and additional bioevents are used.

[5] One hundred and fifty-three samples were processed for foraminifera by standard microfossil techniques for biostratigraphic and paleoenvironmental analyses (with emphasis on paleobathymetric and paleoproductivity proxies). The samples were split (using a microsplitter) into several fractions. Quantitative benthic assemblage and presence/absence biostratigraphic data were compiled from $\geq$63 μm (80,000 foraminifera counted) and $\geq$150 μm (40,000 foraminifera counted) fractions (Figures 2 and 3). The foraminiferal data are expressed as a percentage of the total fauna (percent plankton and percent miliolids) or as a percentage of the benthic rotaliids. The percent planktic (%P*) foraminifera was calculated using the methodology of *van Hinsbergen et al*. [2005], where percent P* is

$$\%P* = 100 * P/(P + B{-}S)), \tag{1}$$

where S = number of stress markers (deep infauna = *Uvigerina* spp. and bolivinids), P = total number of planktics, and B = total number of benthics. Estimates of the paleodepth (Figure 4) were calculated using the equation of *van der Zwann et al*. [1990]:

$$\text{Depth}(m) = e^{3.58718+(0.03534*P)}. \tag{2}$$

[6] The error range on this estimation is a minimum of approximately $\pm$20 m using regional southeast Australian modern analogues [*Smith et al*., 2001; *Smith*, 2002; *Smith and Gallagher*, 2003].

[7] The foraminiferal taxonomy follows that of *Gallagher et al*. [1999], *Gallagher and Holdgate* [2000], and *Li*

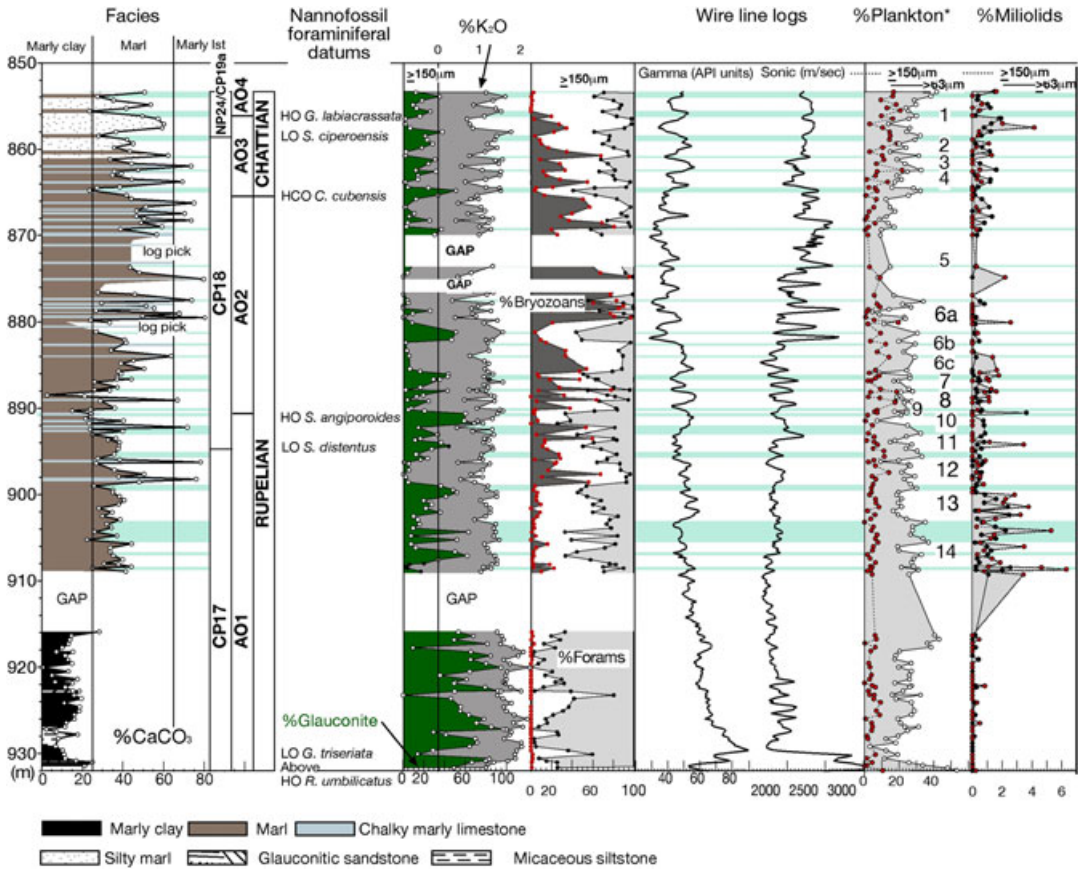

Figure 2. The stratigraphy of the Groper-1 Core, showing facies, biostratigraphy, percent glauconite (dark green graph), bryozoans, and foraminifera from point counts of the ≥150 μm fraction. The percent K_2O is from powdered bulk sediment. The percent forams and bryozoans is a cumulative graph, with the white area denoting all other counted bioclast types. The gamma and sonic logs allow the interpretation of the core gaps. The planktic percentage* is based on *van der Zwann et al*. [1990] and *van Hinsbergen et al*. [2005]. The percent miliolids is expressed as a percentage of the total fauna. Red dots, ≥150 μm; black dots, ≥63 μm. A plankton maximum and highstand (horizontal light green lines) generally mark the top of the numbered units (see Table S4 in the Supporting Information).

and McGowran [2000]. The foraminiferal biostratigraphy follows the Austral realm biozonation [*Huber and Quillevere*, 2005] calibrated to the GTS2004 time scale [*Gradstein et al*., 2004] (Figure 4).

[8] Paleobathymetric and environmental interpretation of the benthic foraminiferal assemblages was based on regional modern analogues, where inner shelf = 0–50 m depth, middle shelf = 50–100 m, outer shelf = 100–200 m, and upper slope = ≥200–500 m [*Li et al*., 1996a, 1996b; *Smith and Gallagher*, 2003; *Smith et al*., 2001] and comparative regional fossil studies [*Holdgate and Gallagher*, 1997; *Li et al*., 2000, 2003; *Gallagher and Holdgate*, 2000; *Gallagher et al*., 2001, 2003; *Gourley and Gallagher*, 2004]. A list of the benthic foraminiferal taxa documented in this work and their interpreted paleoenvironment is available in the Supporting Information, Table S3. The relative abundance of common bioclasts and inorganic clast types (total count = 160,000) were counted in splits of the ≥150 μm fraction to enhance paleoenvironmental and facies analyses (Figure 2). The abundance of bioclasts such as foraminifera, bryozoans, ostracods, echinoderm fragments, and molluscs were counted; these data are expressed as a percentage of the bioclasts counted (Figure 2). Other inorganic components counted in the ≥150 μm fraction include quartz, mica, and glauconite that are plotted as a percentage of the total ≥150 μm fraction. The inorganic clast abundance was compared to elemental data that were obtained from environmental scanning electron microscope (ESEM) analyses. Samples of the powder used in the carbonate analyses were analyzed using the Energy Dispersive Spectrometry (EDS) facility of a Philips (FEI) XL30 at the University of Melbourne. An area of ~400 × 400 μm was scanned (at × 500 magnification) to give semiquantitative "bulk" chemical analysis. While not absolute, the abundance values in the results can be used to chart the relative variability of oxides up a section. The percent K_2O values strongly follow the trends of percent glauconite abundance from ≥150 μm point counts (Figure 2). Where the trends diverge (i.e., where percent glauconite is low and percent K_2O is high), this reflects the presence of abundant <150 μm–sized glauconite (not counted). The data from these analyses can be found inthe Supporting Information, Tables S1–S4).

[9] Stable isotope analyses were conducted out on 79 samples of *Cibicidoides* spp. (primarily *C. perforatus*) to investigate any trends related to global climate variability. Not all horizons yielded sufficiently well-preserved

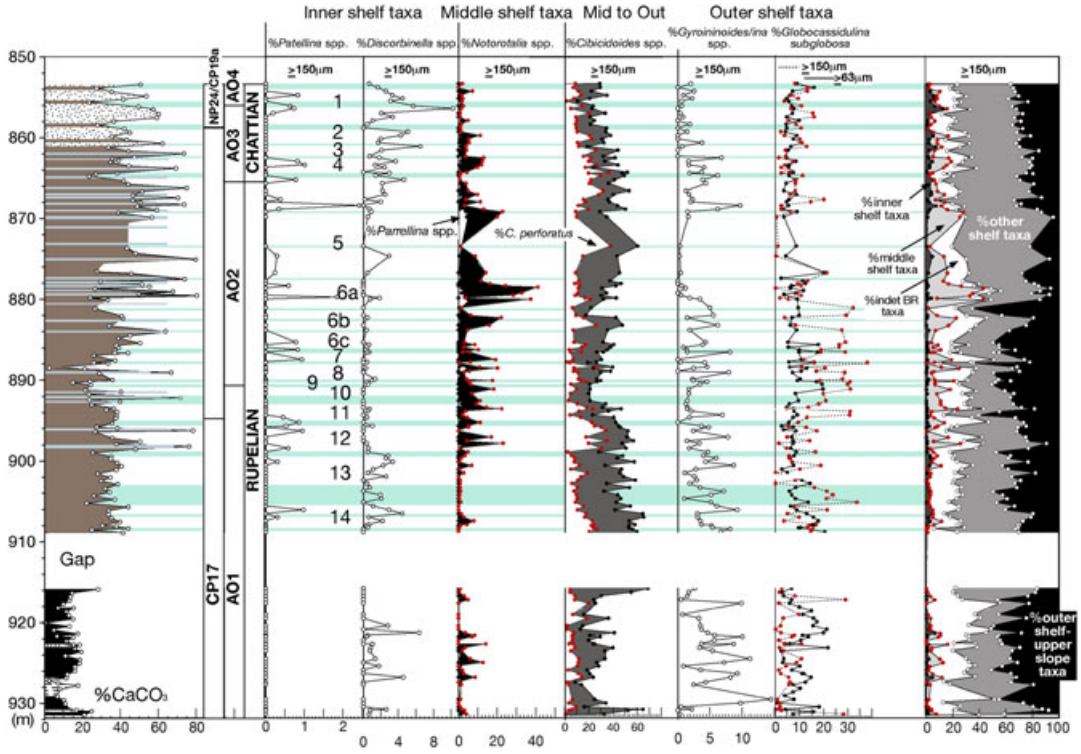

Figure 3. The distribution of common benthic rotaliid taxa (as a percentage of benthic rotaliids [BR]) in Groper-1.

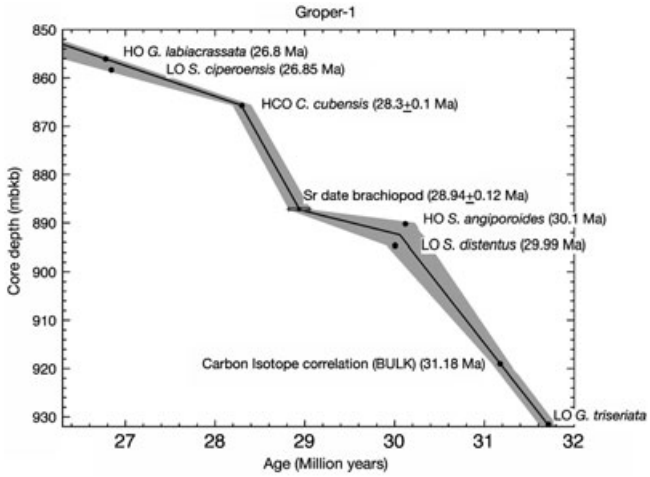

Figure 4. The age depth curve for Groper-1. The error envelope is taken to be ±0.1 Ma, values typical for biostratigraphic data in the Oligocene [*Wade et al.*, 2007].

foraminifera. Out of 153 samples analyzed for foraminifera, only 50 samples yielded sufficient quantities (two to three specimens >150 μm) of well-preserved *Cibicidoides* spp. Visibly altered *Cibicidoides* spp. specimens were extracted from 29 of these samples to investigate the extent of any diagenetic alteration on the assemblage. Stable isotope ratios were analyzed using the MAT253 mass spectrometer at the University of Durham, United Kingdom. Samples were weighed into exetainer vials, with self-sealing septa, which were purged with helium. Phosphoric acid was added manually while the exetainers were held in a block heated to 50°C, and then CO_2 was extracted through a GasBenchII device and introduced to the MAT253. All unknowns were analyzed with international and internal standards of similar weight and were normalized to accepted values for NBS-19 and LSVEC. Isotopic ratios are reported as δ values relative to V-PDB. NBS-18 and the Durham internal standard DCS01 were also measured during each analytical session to monitor performance. The analytical precision (2σ) of replicate analyses of NBS-19 was <0.04‰ for δ^{18}OCIB and δ^{13}CCIB with sample weights of >300 μm, and 0.07‰ and 0.12‰ for δ^{18}OCIB and δ^{13}CCIB when sample weights were <200 μm.

[10] One hundred and fifty three samples of bulk sediment were analyzed for δ^{13}C and δ^{18}O isotopes to create a more detailed isotope record (in the absence of sufficient *Cibicidoides* spp. specimens) and to investigate whether the trends can be used for correlation with other bulk isotope data sets and Oi events. Stable isotope analysis was performed on CO_2 produced by reaction of the calcite powder with 105% phosphoric acid at 70°C. Stable isotope ratios were measured using a GV2003 continuous-flow isotope ratio mass spectrometer at the University of Newcastle, Australia. The results are plotted in per mil (‰) relative to the VPDB using an internal working standard of Carrara Marble (New1) and calibrated using the international standards, NBS18 and NBS19. The analytical uncertainty (2σ) of in-run measurements of Carrara Marble (New1) was 0.08‰ and 0.05‰ for δ^{18}OBULK and δ^{13}CBULK.

[11] One brachiopod sample from log level 827.3 m was dated using strontium isotope analyses. The sample for MC-ICPMS was prepared by removing excess detritus with a microdrill and treated to 10% HCl. It was then transferred to precleaned microcentrifuge tubes and dissolved in 1 mL 8M HNO3. Centrifugation prior to column chemistry revealed complete dissolution, and the samples were loaded onto an 800 µL resin bed of SrSpec resin for extraction chromatography. The column was washed several times with 8M HNO_3 to remove major cations, and Sr was eluted into Teflon vials with 0.005M HNO_3. The $^{87}Sr/^{86}Sr$ ratios were measured by MC-ICPMS at the University of South Carolina. The age was estimated using the strontium curve of *McArthur et al*. [2001] and converted to the GTS2004 time scale [*Gradstein et al*., 2004] using LOWESS V4B look-up table (provided courtesy of John McArthur).

3. Results

3.1. Facies

[12] Three main facies types characterize the section (Figure 2): (1) marly clay, (2) marl alternating with marly limestone/chalk, and (3) silty/sandy marl/limestone.

1. Marly clay facies: dark brown glauconitic clayey marl with rare glauconitic clay (<5% $CaCO_3$) is typical. The glauconite (typically green or dark green) content fluctuates markedly from 28% to 97% (in the ≥150 µm fraction) and 1.2% to 2.2% (bulk) K_2O. Occasional centimeter-scale units are made up of sand-sized dark green glauconite pellets. Many horizons are micaceous (>20%) with up to 2–14% quartz grains in the ≥150 µm fraction. Bryozoans are generally absent; they are rare in basal meter and upper 2 m. Foraminifera make up the majority of the calcareous component with minor bivalves, ostracods, and echinoderm spines. The upper sample of this interval is glauconitic marl followed immediately by a core gap of 7 m. The gamma values are low in this facies at the base and decrease up-section from a maximum of 90 API units at 930 m to 60 API units at 918 m. Above this is a gamma peak followed by an upward decreasing gamma values in the core gap section to 909 m; therefore, there is no appreciable change in facies in this core gap.

2. Marl/marly limestone-chalk cyclic facies: the section from 909 to 861 m is characterized by meter-scale marl and marly limestone (chalk; Figure 2, units 2–14). Foraminifera and ostracods are common, and bryozoans are rare in the brown marl and glauconitic marl in the lower 10 m (units 13 and 14). Glauconite (green/dark green) abundance varies markedly from 60% to 10% (1.4–1% K_2O bulk sediment) in this interval. The lowest unit is not homogenous; there are meter-scale cyclic alternations of centimeter units of bioturbated beige marl (25–30% $CaCO_3$) often overlain by a laminated marl unit and followed by a homogenous brown marl (35–45% $CaCO_3$). The first chalky marly limestone is present at 898 m (at the base of unit 12). Typically these facies are bioturbated, beige-colored bryozoan and spicule-rich wackestone ranging in bed thickness from 0.15 to 0.5 m. In a few horizons the carbonate content of these beige bioturbated facies ranges from 40% to 60% (marl), but most are >65% (marly limestone). The bioturbation takes the form of undeformed oval centimeter-scale patches (often infilled glauconite). These bioturbated facies alternate on a meter scale (0.3–4 m) with homogenous brown bryozoan/shelly or glauconitic marl (25–45% $CaCO_3$). The glauconite and bryozoans show an inverse relationship. Glauconite content varies in abundance from 0% to 60% (with a maximum of 1.3–1.6% K_2O) with peaks every 5–10 m. Bryozoans reach abundances of up to 95% (of the bioclasts) in the marly limestone and range from 20% to 80% in the bryozoan marl (this bioclast is abundant in the interval from 880 to 860 m with common shell horizons and ostracods above 870 m). The upper and lower boundaries between the beige chalky marly limestone and marl are typically gradational and bioturbated. The presence of several marly limestone/marl cycles is inferred in the core gaps between 870 and 882 m by interpreting the gamma, sonic, SP, and SN wireline logs and direct comparison with core/wireline patterns (Figure 2).

3. Silty/sandy marl facies: the upper 8 m (Figure 2, units 1 and 2; Figure 5) of Groper-1 consist of alternations of thick units of beige bioturbated shelly fine sandy limestone/marl (~2 m, 37–60% $CaCO_3$) with thin silty marl units (0.15 m, 24–28% $CaCO_3$). Glauconite abundance fluctuates every 2 m from 0% to 40% (maximum 1.8% K_2O). Bryozoans are not common, reaching a maximum of 34% at 857.55 m and becoming rare up-section.

[13] Thin section analyses and core logging reveal no macroscopic and microscopic facies evidence of subaerial exposure.

3.2. Biostratigraphy and Chronostratigraphy

[14] The age model was constructed using a combination of foraminiferal, nannofossil, and strontium isotope and stable isotope correlations (Figure 4). Planktic foraminifers are common in Groper-1 with an average abundance of 25% fluctuating from a minimum of 5% to >40% (Figure 2). Most specimens are small species of *Globigerina*, *Tenuitella*, *Globorotaloides*, and *Globoturborotalia*. Typical Oligocene species include *Subbotina angiporoides*, *Chiloguembelina cubensis*, and *Globoturborotalia labiacrassata*. These taxa belong to the Austral province described by *Huber and Quillevere* [2005]. The lowest occurrence (LO) of *Guembelitria triseriata* (Figures 2 and 4) near the base of the section suggests the section is younger than 32 Ma [*Li et al*., 2003]. The highest occurrence of *S. angiporoides* at 890.63 m defines the AO1/AO2 zonal boundary at 30.1 Ma [*Wade et al*., 2011]. The highest common occurrence (HCO) of *C. cubensis* at 865.78 m marks the Rupelian/Chattian boundary and the top of the AO2 Zone at 28.3 Ma [*Wade et al*., 2011]. The highest occurrence of *Globoturborotalia labiacrassata* at 856.18 m denotes the AO3/AO4 zonal boundary dated at 26.8 Ma [*Gradstein et al*., 2004; *Huber and Quillevere*, 2005].

[15] Moderately to well-preserved nannofossils are common. The nannofossil biostratigraphic zonation is based on *Martini* [1971], *Okada and Bukry* [1980], and secondary bioevents. The assemblage lacks *Reticulofenestra umbilicus* (Figure 2), suggesting the base of the section is younger than its highest occurrence (HO) at the base of Zone NP 23, early Oligocene (<32.3 Ma in the low to middle latitudes) [*Berggren et al*., 1995]. This concurs with foraminiferal evidence suggesting that the base of the section is

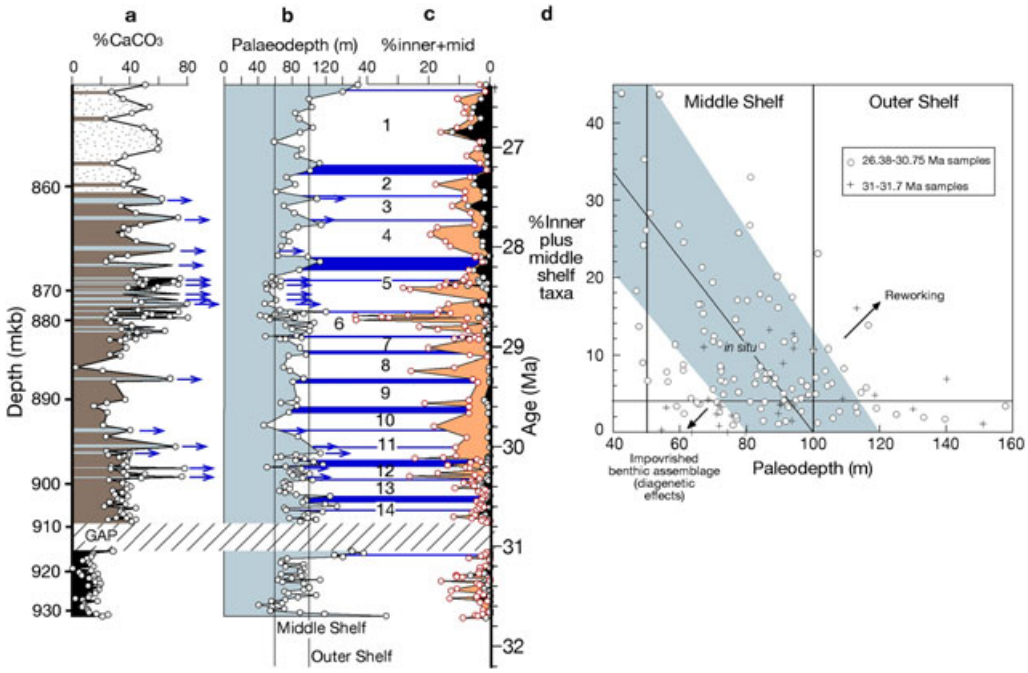

Figure 5. Paleodepth in Groper-1 plotted using the age model of Figure 4. (a) Facies. (b) Paleodepth calculated from percent plankton* (≥63 μm). The blue arrows are chalky marl horizons not processed for foraminifera (due to strong induration), or they underrepresent planktic abundance (sea level) due to diagenesis. (c) The percent inner (black) and middle (orange) shelf taxa (≥150 μm). Units 1–14 are characterized by a shallower section (white) overlain by a highstand (deeper) interval (dark blue). (d) A plot showing the relationship between the percent inner plus middle shelf benthic rotaliid taxa (≥150 μm) versus the paleodepth calculated from percent plankton (≥63 μm). The light blue interval incorporates the paleodepth error estimate of ±20 m.

younger than 32 Ma. The presence of few to common *Sphenolithus predistentus* and rare *Sphenolithus distentus* also confirms an NP 23 Zonal age for most of the section. Additional important markers, such as *Chiasmolithus altus* (the last representative of the genus *Chiasmolithus* in the Oligocene) and *Cyclicargolithus abisectus* >10 μm are present. These taxa first occur at the base of the Zone NP 23 [*de Kaenel and Villa*, 1996; *Villa et al*., 2008] and range into the late Oligocene. The LO of *Sphenolithus distentus* at 894.74 m marks the CP17/18 boundary [*Okada and Bukry*, 1980]. However, this LO should be considered with caution, first because the distribution of this species in the section is discontinuous, and the variable preservation of the assemblage may have prevented the preservation of older specimens, and secondly because this species has been matter of taxonomic discussion among the specialists; some authors consider the oldest specimens to be transitional forms to *S. predistentus*. However, *Olaffson and Villa* [1992] and *Blaj et al*. [2009] identified distinctive forms of *S. distentus* first appearing at 30.62 and 29.99 Ma, respectively. The LO of *S. distentus* in the section at 890.74 m is very close to the *S. angiporoides* datum at 890.63 m confirming this 4 m section is likely to be 30 Myr old. At 858.47 m the LO of *Sphenolithus ciperoensis* defines the base of the Zone NP 24. The LO for *S. ciperoensis* has recently been recalibrated (using the ODP Site 1218 astronomical calibration) by *Blaj et al*. [2009] to 27.142 Ma (27.175 Ma; see *Gradstein et al*. [2004]. This is followed by the HO of *G. labiacrassata* at 26.8 Ma [*Gradstein et al*., 2004] at 856.18 m.

[16] Three $^{87}Sr/^{86}Sr$ values were obtained for one brachiopod at 827.3 m. A total age range of 28.68–29.4 Ma (with 2σ errors) was estimated for the three values using the strontium curve of *McArthur et al*. [2001] converted to *Gradstein et al*. [2004] time scale using LOWESS V4B look-up table. Using the least squares method, this yielded an age of 28.94 ± 0.12 Ma (2σ±).

[17] The δ^{13}CBULK isotope positive excursion at 920 m is correlated to a positive isotope excursion in δ^{13}CBULK data from ODP Site 1218 [*Pälike et al*., 2006] and ODP Sites 689 and 690 [*Shackleton and Hall*, 1990] converted to the GTS2004 time scale at ~31.18 Ma (Figure 4).

3.3. Foraminiferal Distribution

[18] Planktic foraminifera are relatively rare in the >150 μm fraction ranging from 0% to a maximum of 20% in the upper half of the section (Figure 2). Planktic foraminifera are more common in the ≥63 μm fraction (i.e., smaller planktic forms dominate). Values fluctuate markedly up-section from maxima of 30% to 60% to <10%. In general, planktic foraminifera are relatively common in the chalky marly limestone and lower carbonate marl facies (percent $CaCO_3$ < 30%) compared to higher carbonate marl facies (percent $CaCO_3$ values ≥ 30%). Plankton peaks occur when middle and inner shelf rotaliids and miliolids taxa are typically at their minima, above 910 m several units with this pattern can be distinguished (units 1–14; Figures 2, 3, and 5) this suggests a depth control on plankton distribution (Figure 5). It was not always possible to get sufficient counts in some of the highly

indurated chalky units; these facies typically contain common planktic foraminifera in thin section.

[19] Miliolids are rare. They become more common above 909 m (~30.75 Ma) where taxa such as *Quinqueloculina* spp. and/or *Triloculina* spp. are present in the majority of samples. The abundance of these taxa fluctuate markedly from 0% to maxima of 3 to >6% in the 63 and 150 μm fractions above 909 m (Figure 2). Inner shelf foraminifera (mainly *Discorbinella* spp., Figure 3) make up a minor part of the benthic rotaliid assemblage. Moderate peaks of 4–6% are present, reaching a maximum of 12% at around 856 m (26.8 Ma). Other inner shelf taxa present include *Discorbis* spp., *Spirrilina* spp., *Patellina* spp., *Rosalina* spp., and *Wadella globiformis*. Middle shelf assemblages (≥150 μm) in the section (Figure 3) are dominated by *Notorotalia* spp. with minor *Parrellina* spp. and *Pullenia quinqueloba*. Middle shelf taxa are relatively uncommon (0–15% of the benthic rotaliids) below 893 m (30.08 Ma). Strong fluctuations from 25% to 5% are apparent above this level (units 1–12). Middle shelf species reach a maximum of 45% of the benthic rotaliids around 880 m (28.72 Ma). Above 870 m (28.43 Ma), middle shelf taxa abundance varies markedly from 15% to 1%. Outer shelf taxa dominate the benthic rotaliid assemblage (forming between 40% and 60%: ≥150 μm). The middle to outer shelf *Cibicidoides perforatus* and *Cibicidoides* spp. are most common comprising (on average) 30% of the benthic rotaliids; these taxa reach up to 50% of the total rotaliids (Figure 3). Other common species in the ≥150 μ m fraction include *Globocassidulina subglobosa*, *Gyroidinoides* spp., and *Cassidulinoides* spp. Other important yet minor components of this outer shelf assemblage include *Anomalinoides macroglabra*, *Heterolepa* spp., *Lenticulina* spp., *Pullenia bulloides*, *Sphaeroidina bulloides*, and *Astrononion* spp.

3.4. Paleodepth, Back Stripping, and Sea Level Change

[20] There is a negative correlation (-0.5) between the increasing paleodepth (calculated from percent plankton*) and decreasing percent inner plus middle shelf taxa (Figure 5). The relationship is likely to be complicated by bioturbation processes causing assemblages mixing (reworking). In addition, a diagenetic bias, especially in the indurated chalk facies, has resulted in underestimations of the percent planktic in the assemblages (dark blue arrows on Figure 5). Reworking by paleocurrent processes is not likely to have caused assemblage mixing, as the sequence is dominated by low-energy facies (chalk and marl). Based on the data in Figure 5, we interpret the calculated paleodepths (from percent plankton*) to reflect relative sea level change (Figure 5a), and this variability has at least a ±20 m depth error. The succession was 1-D Airy back-stripped using OSXBackstrip using the algorithms and formulas of *Allen and Allen* [1990] and *Watts* [2001] to remove the thickness of accumulated sediment and compaction effects. OSXBackstrip calculates *R*1 (the first reduction of the back-stripping method) of *Kominz et al.* [2008] representing the water depth above basement without sediment (the input parameters used to calculate this are in the Supporting Information, Table S5). *R*1 is then used to calculate *R*2 (the second reduction is regional sea level change derived from paleodepth estimates in the absence of tectonics; see output data in the Supporting Information, Table S6) of *Kominz et al*. [2008]:

$$R2 = (R1 - \mathrm{TS})\left(\frac{\rho a - \rho w}{\rho a}\right), \quad (3)$$

where TS = tectonic subsidence, estimated by fitting a regional cooling plate model to *R*1. Also, ρa = asthenosphere density (3300 kg/m^3) and ρw = water density (1000 kg/m^3). The tectonic subsidence (TS) component was estimated from two modeled thermal subsidence curves of this passive margin region [*Hegarty et al*., 1986; *Rahmanian et al*., 1990] using a stretching factor of 1.4 and a 15 Ma rifting time from 95 to 80 Ma. The regional curves show consistent thermal subsidence during the late Paleogene of ~10 m/Myr in the absence of any major tectonic events. In addition to the errors in paleodepth input into our sea level curve, if subsidence was slower or faster in this region, this would also influence the long-term trends of the sea level variation; however, it would not alter the strong shorter-term variability of our record nor its magnitude. The resulting derived sea level curve (Figure 6b), hereafter called the Gippsland sea level (GSL), for Groper-1 shows similar magnitudes to the New Jersey sea level curve (NJSL) generated by *Miller et al*. [2005] and *Kominz et al*. [2008]. The trend of NJSL is overprinted by long-term mantle dynamic contamination that contributes to a 50–100 m fall [*Moucha et al*., 2008] over the last 30 Myr (Figure 6). It is also important to consider our eustatic estimates in the context of the dynamic topography of southeast Australia during the Oligocene. It is possible that variations in dynamic topography account for some of our long-term sea level variability. *Heine et al*. [2010] has reconstructed the dynamic topography of Australia for various time slices for the last 70 Myr. Their paleogeographic reconstruction for Oligocene suggests dynamic subsidence of ~20 m from 30 to 26 Ma (Figure 6). The dynamic contribution to subsidence for GSL and NJSL is clearly overprinted by a rapid sea level variations ranging from -30 to +50 m.

3.5. Oxygen Isotopes

[21] The *Cibicidoides* spp. δ^{18}OCIB values were adjusted to seawater equilibrium values by adding +64‰ [cf. *Wade and Pälike*, 2004]. All other values were not adjusted. The *Cibicidoides* spp. δ ^{8}OCIB values (Figure 6e) are variable, and the majority lie within the range of published compilations for the early Oligocene [*Zachos et al*., 2008; *Cramer et al*., 2009]. Some of the δ^{18}OCIB values are strongly negative, less than -1.5‰, suggesting some diagenetic alteration of the foraminifera. However, the majority of the visibly altered and "fresh" *Cibicidoides* spp. specimens yield similar δ^{13}C and δ^{18}O values, suggesting only minor diagenetic effects on the benthic isotope pattern (Figure 6). The δ^{18}OCIB values below 29 Ma are negative with three positive excursions at ~29.7, 30.3, and 31.3 Ma. Above 29 Ma, values are positive with three positive δ^{18}OCIB excursions at ~27.4, 28, and 28.5 Ma. Two δ^{18}OBULK positive excursions are present between 31.1 and 31.5 Ma, separated by an interval of negative values. Above 30.4 Ma, δ^{18}OBULK values are generally negative with positive excursions at 30.4, 30, ~29.6, and 29.2 Ma, from 28.9 to 28.6 Ma, and at 28.3 Ma. Above 28.3 Ma, there are upward decreasing variable negative δ^{18}OBULK values.

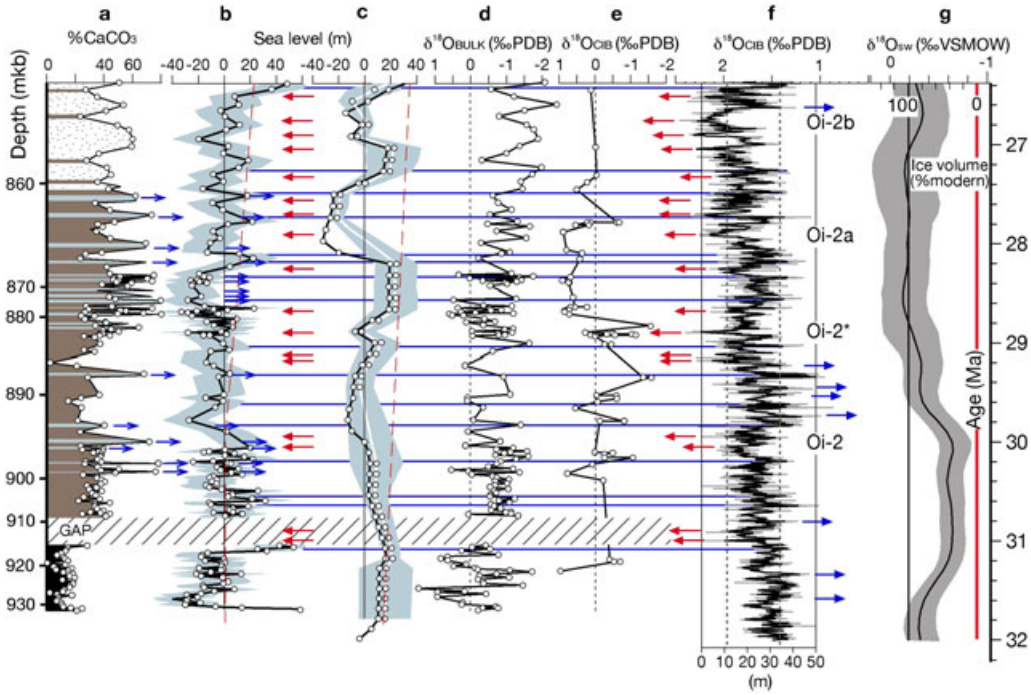

Figure 6. Sea level in Groper-1. (a) Facies. (b) The Gippsland Sea Level (GSL) curve (with error) derived from back-stripping the succession using paleodepths (see derivation in the Supporting Information, Table S6); the blue arrows are chalky marl horizons not processed for foraminifera (due to strong induration), or they underrepresent planktic abundance (sea level) due to diagenesis. A possible dynamic subsidence trajectory (dashed red line) is shown [*Heine et al*., 2010]. (c) the New Jersey Sea Level curve of *Miller et al*. [2005] (black) and that of *Kominz et al*. [2008] (white with error range). A possible dynamic subsidence trajectory (dashed red line) is indicated [*Moucha et al*., 2008]. (d) Bulk and (e) *Cibicidoides* spp. oxygen isotope data. (f) Isotope data (gray) from Site 1218 (adapted from *Pälike et al*. [2006] using the *Gradstein et al*. [2004] time scale with a three point running average; black line); the relative sea level change values are based on a 0.24‰/10 m sea level (0.16‰/10 m ASL, or apparent sea level) amplitude estimate of *Pekar et al*. [2006] for this site. The horizontal blue lines represent isotopic minima (probable interglacials/terminations) that correlate with GSL highstands; the blue arrows indicate terminations not represented in Groper-1.The red arrows are glacial/isotopic maxima. (g) Estimates of the isotopic composition of sea water and ice volume showing an error envelope (gray) [*Cramer et al*., 2011].

4. Interpretation

4.1. Sea Level Change

[22] The dominance of clayey marl/marl and chalky marl (wackestone) suggest the low-energy (below wave base) condition prevailed. Modern calcareous mud facies in the Gippsland region typically accumulates below 100 m [*Smith and Gallagher*, 2003], deeper than 180 m in the Otway Margin southeast Australia [*Boreen et al*., 1993] and below 80 m in the Great Australian Bight [*James et al*., 2001]. Oligocene bryozoan marls are interpreted to have been deposited in middle to outer shelf environments in the Otway Basin southeast Australia [*Gallagher et al*., 1999], where these facies formed in shallower conditions compared to today, because the Southern Ocean was narrower with a reduced fetch, creating a shallower (paleo) wave base. Other Paleogene mudstone/marl facies in southeastern United States are interpreted to reflect deposition in open shelf conditions below storm wave base (>100 m depth); however, some of these facies may have formed in shallower more sheltered conditions [*Coffey and Read*, 2004]. The presence of abundant glauconite at regular intervals suggests periods of slow sedimentation in open marine conditions [*Odin and Fullagar*, 1988] at depths between 70 and 500 m. Depth estimates from the percentage of planktic foraminifera in the sequence [*van Hinsbergen et al*., 2005, Figure 5] vary from outer shelf depths (>100 m) to middle shelf depths (>50 m) with few samples shallower than 50 m. This depth range concurs with the benthic foraminiferal assemblage data that is dominated by middle to outer shelf species with minor inner shelf taxa (Figures 3 and 5). The percent inner and middle shelf taxa (Figure 5), the abundance of inner shelf miliolids (Figure 2), the percentage of planktic foraminifera, oxygen isotope values, and facies can be used to interpret sea level variability (Figure 6). In addition, back-stripped data (Figure 6b) show sea level change amplitudes in the section are comparable with NJSL (Figure 6c) [*Miller et al*., 2005; *Kominz et al*., 2008].

[23] The lower clayey marl facies from 31.1 to 31.7 Ma with minor middle and inner shelf taxa are interpreted to have been deposited in low-energy middle to outer shelf environments (70 to >100 m), representing a sea level variability from -25 to +50 m (Figure 6b). From 30.3 to 30.8 Ma, marl facies shallows from outer shelf to middle shelf up-section with several deeper outer shelf (>100 m)

transgressive events, varying from maximum of -20 to +35 m. The first chalky marl/marly limestone facies at 30.3 Ma marks the beginning of a period of strong sea level variability. Above this level, meter-scale cycles of middle shelf marl (50–90 m paleodepth) alternate with outer shelf (>100 m) chalk or marl, representing sea level fluctuations ranging from ±25 m. Several shallowing events are associated with positive oxygen isotope excursions at 30.3, 29.7, 29.2, 28.6, and 28 Ma (Figures 6a, 6d, and 6e). The GSL values can be directly compared to the magnitude of *Cibicidoides* spp. δ^{18}OCIB variability (Figure 6e, especially 27.8–28 Ma), suggesting a 0.5‰ oxygen isotope change is equivalent to 10 m sea level change. The chalk/marl cycles disappear above 27.5 Ma to be replaced by meter-scale alternations of outer shelf marl (>100 m) and middle shelf (>60 m) silty marl, representing sea level fluctuations of ±20 m culminating in deepening to more than +50 m by 26.4 Ma.

4.2. Paleoclimate

[24] The succession is dominated by small (<150 μm), temperate middle- to high-latitude Austral Province planktic foraminiferal taxa *sensu* [*Spezzaferri et al*., 1991; *Huber and Quillevere*, 2005]. In addition, warm-water nannofossil *Discoaster* and *Sphenolithus* [cf. *Chepstow-Lusty et al*., 1992] are relatively rare, and the latter represented by several low- to medium-latitude species. The nannofossil and foraminiferal data suggest cool to temperate oceanic conditions with no warming events or warm-water microfossil migrations.

5. Discussion

[25] The Oligocene of Groper-1 was deposited in middle to outer shelf cool-temperate conditions from 26.7 to 31.5 Ma at a paleolatitude of 55°S [*Stickley et al*., 2004, Figure 1]. The sequence is characterized by a large variations in sea level that we interpret to reflect processes associated with Oi glacial events previously interpreted from deep-sea oxygen isotope data [*Miller et al*., 1991; *Pekar and Miller*, 1996; *Wade and Pälike*, 2004; *Pälike et al*., 2006] and from stratal geometries on the New Jersey Coastal Plain [*Pekar et al*., 2002, 2006]. The dominant meter-scale marl/chalk couplets are interpreted to be primary dilution cycles [cf. *Boulila et al*., 2010; *Westphal et al*., 2010]. During lower sea level, higher siliciclastic input resulted in marl (>30% $CaCO_3$) deposition at depths from 70 to 50 m. Relative sea level rise to >100 m resulted in chalk deposition as the area moved away from the source of siliciclastics [cf. *Swart*, 2008]. However, not all the higher sea level events resulted in chalk facies deposition; some of the clayey marl and the majority of the marl facies (with <30% $CaCO_3$) formed in outer shelf depths.

5.1. Oligocene Glacial and Interglacial Sea Level

[26] We use our data set and its similarity to NJSL [*Miller et al*., 2005; *Kominz et al*., 2008] and the stable isotope data of ODP Site 1218 [*Wade and Pälike*, 2004; *Pälike et al*., 2006] to identify Oi glacial maxima (Oi-2 [~30 Ma], Oi-2* [~29 Ma], Oi-2a [~28 Ma] and Oi-2b [~27 Ma]; red arrows in Figure 6) and a series of deglaciations (terminations, dark blue arrows, and horizontal lines in Figure 6). Oi periods are thought to have been driven by 1.2 Ma obliquity cyclicity [*Wade and Pälike*, 2004; *Pälike et al*., 2006]. The previously recognized Oi "events" probably represent glacial maxima where eustatic falls exceeded 30 m when the size of the EAIS was greater than or equal to today [*Pekar and Christie-Blick*, 2008]. Where our isotopic data have sufficient resolution, relatively low sea level estimates in our section are found to coincide with heavier foraminiferal oxygen isotope values. Furthermore, the majority of interglacial events (lightest isotope values in Figure 6f) at Site 1218 correlate with the highest sea level estimates and/or outer shelf chalk facies in G-1 (Figures 6a and 6b). In particular, the GSL closely resembles NJSL after 27.5 Ma. These patterns indicate that the G-1 section reflects late Oligocene glacioeustasy and that the GSL represents an additional relative sea level record to NJSL that may be used to infer aspects of early EAIS and sea level dynamics previously addressed using isotopic data [*Gasson et al*., 2012].

[27] The NJSL and GSL curves, while similar, show variations that might reflect regional allocyclic stratigraphic variability (the former is a siliciclastic dominated sequence, and the latter carbonate rich); errors in paleodepth estimates (more than ±20 m); and errors due to reworking or diagenetic alteration and errors in chronology (error ranges of ±0.1 to ±0.5 Ma are possible in both sections). The NJSL record is also biased, as lowstand deposits are generally absent in the New Jersey Shelf succession [*Kominz et al*., 2008], whereas in G-1 the strata have not been exposed to subaerial emergence resulting in the deposition of lowstand marl facies; hence the GSL estimates would potentially reflect sea level lows during the Oligocene. The differences between sections may also reflect temporal variations in the dynamic topography [*Heine et al*., 2010; *Moucha et al*., 2008] although the subsidence rate for each section is similar, especially after 30 Ma, and the pattern of sea level change has a much higher temporal resolution. The sea level variation between sections might also be due to the glacial isostatic adjustment (GIA) response to glacial maxima and minima [*Farrell and Clark*, 1976; *Bassett et al*., 2005; *Bamber et al*., 2009] between our near-field 55°S paleolatitude GSL and the far-field 35–40°N paleolatitude NJSL [*Kominz et al*., 2008] (Figure 7). GIA effects typically result in strongly diachronous sea levels. During Oi glacial maxima, the volume of the EAIS is estimated to have been between 100% and 140% of its present volume [*Pekar and Christie-Blick*, 2008; *Cramer et al*., 2011]; this would have resulted in a peripheral bulge near Antarctica [*Clark et al*., 1978], lowering sea level in G-1 and increasing sea level in NJ (Figure 7a). This is called antisiphoning [*Clark et al*., 2009] and is the process where a proximal bulge caused by ice sheet expansion on the Antarctica margin pushes (or siphons) water from the near field into the far-field ocean. This diachronous sea level variability would have been most pronounced during Oi maxima, when the EAIS may have been 140% of present. During Oi interglacials when EAIS ice volumes were 40–60% of present [*Pekar and Christie-Blick*, 2008; *Cramer et al*., 2011] rebound, subsidence and ocean siphoning (Figure 7b) [*Mitrovica and Milne*, 2002] would have caused higher sea levels immediately after terminations in NJ (far field) and lower values in G-1 (near field) before equilibrating to higher values in G-1 compared NJ (Figure 7b). Another effect that would lower sea level at continental margins may have been continental levering [*Mitrovica and Milne*, 2002; *Walcott*, 1972], as increased water loading during interglacials may have lowered sea level (Figure 7c).

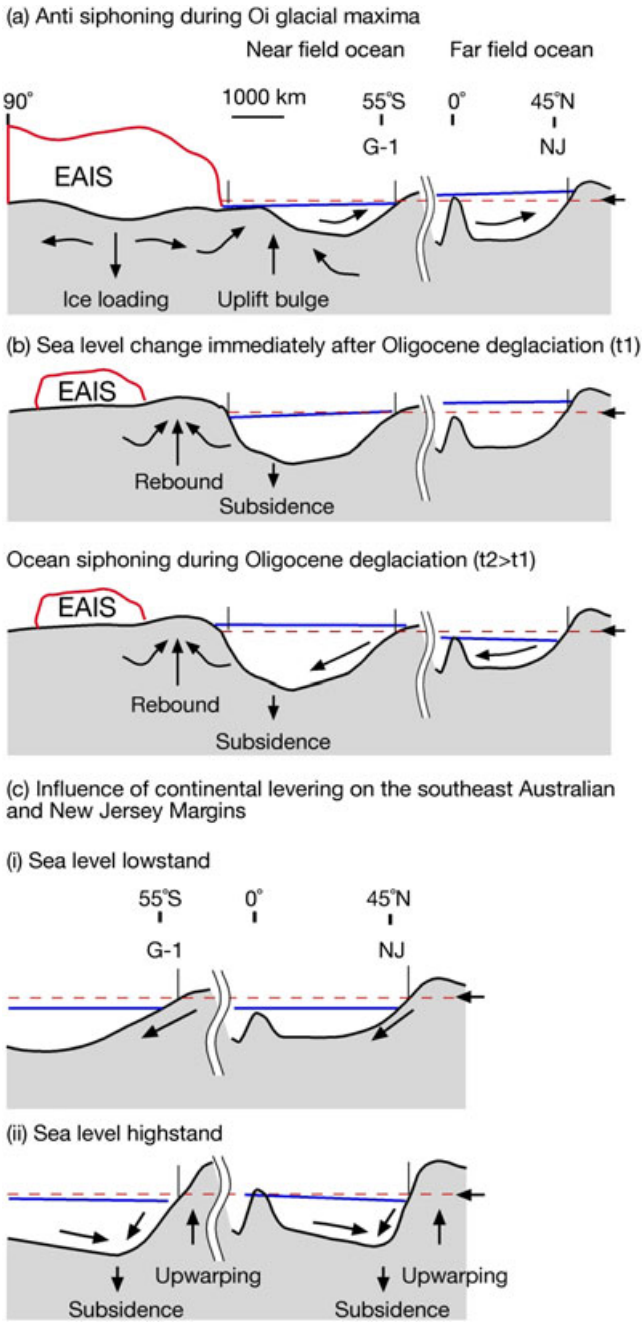

Figure 7. Likely GIA controls on Oligocene relative sea level. The area between 90° and 55°S (G-1) is to approximately to scale; the blue line is relative sea level with respect to a datum (red dashed line), and the far-field ocean is not to scale. Not to scale vertically. (a) An Oi glacial maximum with the EAIS at 100% of present. Antisiphoning [*Clark et al*., 2009] reduces sea level at G-1 while increasing sea level at NJ. (b) Oi interglacial when the EAIS is 50% of present. Ocean siphoning [*Mitrovica and Milne*, 2002] initially increases sea level in NJ compared to G-1 (t1) followed by higher sea levels in the near-field ocean compared to the far field (t2). (c) Continental levering [*Walcott*, 1972] may act to reduce relative sea levels in continental margin regions like NJ and G-1 during deglaciations. Diagrams adapted from *Gornitz* [2009].

[28] Notwithstanding the potential (often similar) errors above in the two relative sea level records, it is likely that the signal preserved in the GSL reflects a near-field ocean response to East Antarctic Ice Sheet dynamics and the NJSL a far-field response (in the absence of any other significant ice sheets during the Oligocene). With this in mind, a few comparisons can be made between the two sections during Oligocene glacial maxima and minima.

[29] Glacial/isotopic maxima (red arrows in Figure 6) are associated with lower sea levels (-30 to <0 m) in GSL and NJSL after 29.4 Ma, when average EAIS volume expanded to ≥100% of present (Figure 6g). Prior to this time, EAIS estimates are a low as 40% and the eustatic pattern is not as pronounced (especially in NJSL). Three Oi glacials are expressed in the NJSL record; these have equivalent events in the GSL curves. The Oi-2 (~28.85 Ma) sea level minimum of (greater than -10 m) in NJSL has an equivalent lowstand of less than -20 m in GSL; this >10 m variation might be evidence of antisiphoning effects (Figure 7). The lowstand estimates for Oi-2b in the NJSL are 10 m lower than the GSL; the reason for this is not clear, although the lack of lowstand deposition in the NJSL is likely to increase errors in these depth estimates, so the values cannot be compared [*Gasson et al*., 2012].

[30] In both records, Oi-2 isotopic maxima at ~30 Ma are not well expressed. In the NJSL this lowstand is not likely to have been fully sampled and may lie within the error range of the biostratigraphy. In G-1, two lowstand marl units interbedded with a highstand chalky marl are present at ~30 Ma, suggesting the GSL section may cover this interval; however, the upper Oi-2 maximum is not sampled and the lower Oi-2 maximum occurs in the 100 kyr biochronological error range. The isotope maxima around 31 Ma are not sampled in GSL and unrepresented in NJSL.

[31] Interglacials/isotopic minima (dark blue horizontal lines and arrows in Figure 6) are associated with higher sea levels (more than +10 to 20 m). From 29.4 to 30.7 Ma, GSL highstands are on average ~10 m higher than the NJSL record, within the range of error estimates for the section; however, the persistence of this pattern for 1.3 Ma might also be related to ocean siphoning effects (Figure 7) during a series of deglaciations when the EAIS may have contracted to 40% of present. The pattern of interglacials is more pronounced after 29.4 Ma in the GSL, where each event correlates to isotopic minima in the Site 1218 data (Figure 6f). However, there are many more highstand events preserved in the GSL compared to the NJSL, so GIA effects are hard to decipher. Overall the highstand events in the GSL exceed the sea level in the equivalent NJSL section and probably indicate the prevalence of ocean siphoning in this period of rapidly fluctuating EAIS volume.

5.2. East Antarctic Ice Sheet Instability

[32] The GSL record shows sea level variability of ±25 m was a persistent feature during the Oligocene (Figure 6) and that the EAIS contracted and expanded to between 40% and 140% of its present size many times. The pattern and intensity of the sea level variability in the GSL is comparable to oxygen isotope variability in Site 1218, where the majority of highstand/lowstand units in the GSL have corresponding isotopic minima/maxima. The strong correspondence between these two separate proxy data sets suggests that

the early EAIS expanded and contracted through a several glacial and interglacial events. The oxygen isotope data from ODP Site 1218 (Figure 6f) suggest that the glacials lasted 100–200 kyr and were followed by short-lived interglacials. The lack of a consistent pattern (or symmetry similar to the Pleistocene glacial cycles) to the glacial expansions and contractions indicates that the EAIS was highly unstable. The magnitude of the cyclicity increases after 30 Ma, associated with an overall shift in EAIS volume (100–140% of present; Figure 6g) [*Cramer et al*., 2011], suggesting that even as the EAIS built up it remained highly unstable.

[33] When our data are compared to CO_2 estimates for the Oligocene, it is evident that EAIS instability occurred when levels were similar or ~200 ppmv higher than present [*Beerling and Royer*, 2011; *Pagani et al*., 2005]. Estimates higher than 600 ppmv are similar to those projected by *Solomon et al*. [2007] for 2100. This suggests the intriguing possibility that the present EAIS may become susceptible to instability with future climate change. *Pollard and DeConto* [2005] were unable to model this level of Oligocene EAIS instability due to a hysteresis affect, suggesting either pCO_2 changes were greater than previously estimated or the EAIS was more unstable than the modeled results suggest.

6. Conclusions

[34] The integration of microfossil, facies, benthic foraminiferal (*Cibicidoides* spp.), and bulk $\delta^{18}O$ isotope analyses on a subsurface carbonate sequence in southeastern Australia has revealed a 5 million year old record of Oligocene cool, temperate, high-paleolatitude (55°S) sea level variability. Clayey marl, marl, and chalky marl dominate in the absence of evidence for subaerial exposure. The facies were deposited below wave base in low-energy conditions at middle (50–100 m) to outer shelf (>100 m) paleodepths. The facies is strongly cyclic, reflecting strong sea level variability. Back-stripping estimates has produced the Gippsland Sea Level curve (GSL), showing persistent sea level variability of $\pm$25 m (from -30 to +50 m), with highstand and lowstand facies corresponding to isotopic maxima and minima in Site 1218. The early Oligocene was characterized by 100–200 kyr glacials alternating with shorter interglacials due to high EAIS instability (fluctuating from 140% to 40% of its present volume). The magnitude and intensity of these cycles were accentuated after 30 Ma, when the EAIS reached close to its present volume. The NJSL and GSL show many similarities, especially from 29 to 26.4 Ma; however, there are resolution differences and mismatches that may be accounted for by errors in biochronology, paleodepth estimates, taphonomic processes, and the relative lack of lowstand deposits used to construct the NJSL (these appear to be present in the GSL). Notwithstanding these possible errors, GIA processes such as interglacial ocean siphoning and glacial antisiphoning are likely to have caused diachronous sea level rises and falls in the near-field GSL and the far-field NJSL. Modeling of these processes is likely to yield further insights in Oligocene glacioeustatic and isostatic dynamics.

[35] **Acknowledgments.** We are grateful to Paul Pearson (Cardiff University), Michelle Kominz, and an anonymous reviewer for their constructive reviews of this paper. We thank Mike Wiltshire (Occam Technology), who donated the wireline log data. This research was partly supported by ARC DP0558150 (M.W. and S.G.). Wiltshire Geosciences donated the wireline log data. DPI Victoria (Terry Smith) and ESSO Australia (Adem Djakic) are to be thanked for allowing access to the Groper-1 core. We are grateful to Colin MacPherson and Joanne Peterkin for stable isotope analyses at Durham University, which were funded by a Natural Environment Research Council (NE/G014817/1) grant to B.W.

References

Allen, P. A., and J. R. Allen, (1990), Basin Analysis, Principles and Ppplications, 451 pp., Blackwell Sci., Oxford, U. K.

Bamber, J. L., R. E. M. Riva, B. L. A. Vermeersen, and A. M. LeBrocq (2009), Reassessement of the potential sea-level rise from a collapse of the West antarctic Ice Sheet, *Science*, *324*, 901–903.

Barrett, P. J., (1989), Antarctic Cenozoic History From CIROS-1 Drillhole, McMurdo Sound, 254 pp., Dep. of Sci. and Ind. Res., Sci. Publ. Cent., Wellington, New Zealand.

Bassett, S. E., G. A. Milne, J. X. Mitrovica, and P. U. Clark (2005), Ice sheet and solid earth influences on far-field sea-level histories, *Science*, *309*, 925–928.

Beerling, D. J., and D. L. Royer (2011), Convergent Cenozoic CO_2 history, *Nat. Geosci.*, *4*, 418–420.

Berggren, W. A., D. V. Kent, C. C. Swisher, and M. Aubry (1995), Revised Cenozoic geochronology and chronostratigraphy, in Geochronology, Time Scales And Global Stratigraphic Correlation, edited by W. A. Berggren et al., pp. 129–212, Soc. for Sediment. Geol., Tulsa, Okla.

Blaj, T., J. Backman, and I. Raffi (2009), Late Eocene to Oligocene preservation history and biochronology of calcareous nannofossils from paleo-equatorial Pacific Ocean sediments, *Rivista Ital. Paleontol. Stratigr.*, *115*, 67–85.

Boreen, T., N. P. James, D. Heggie, and C. Wilson (1993), Surficial cool-water carbonate sediments on the Otway continental margin, southeastern Australia, *Mar. Geol.*, *112*, 35–56.

Boulila, S., M. de Rafelis, L. A. Hinnov, S. Gardin, B. Galbrun, and P.-Y. Collin (2010), Orbitally forced climae and sea-level changes in the Paleoceanic Tethyan domain (marl-limestone alternation, lower Kimmeridgian, SE France, *Palaeogeogr. Palaeoclimatol. Palaeoecol.*, *292*, 57–70.

Chepstow-Lusty, A., J. Backman, and N. J. Shackleton (1992), Comparison of Upper Pliocene Discoaster abundance variations from the Atlantic, Pacific and Indian Oceans: The significance of productivity pressure at low latitudes, *Mem. Sci. Geol.*, *44*, 357–373.

Clark, J. A., W. E. Farrell, and W. R. Peltier (1978), Global changes in Postglacial sea level: A numerical calculation, *Quat. Res.*, *9*, 265–287.

Clark, P. U., J. X. Mitrovica, G. A. Milne, and M. E. Tamisiea (2009), Sea-level fingerprinting as a direct test for the source of global meltwater pulse IA, *Science*, *295*, 2438–2441.

Coffey, B. P., and J. F. Read (2004), Mixed carbonate-siliciclastic sequence stratigraphy of a Paleogene transition zone continental shelf, southeastern USA, *Sediment. Geol.*, *166*, 21–57.

Cramer, B. S., J. R. Toggweiler, J. D. Wright, M. E. Katz, and K. G. Miller (2009), Ocean overturning since the Late Cretaceous: Inferences from a new benthic foraminiferal isotope compilation, *Paleoceanography*, *24*, PA4216, doi:10.1029/2008PA001683.

Cramer, B. S., K. G. Miller, P. J. Barrett, and J. D. Wright (2011), Late Cretaceous–Neogene trends in deep ocean temperature and continental ice volume: Reconciling records of benthic foraminiferal geochemistry ($\delta^{18}O$ and Mg/Ca) with sea level history, *J. Geophys. Res.*, *116*, C12023, doi:10.1029/2011JC007255.

de Kaenel, E. and G. Villa, (1996), Oligocene-Miocene calcareous nannofossil biostratigraphy and paleoecology from the Iberia abyssal plain, *Proc. Ocean Drill. Prog. Sci. Results*, *149*, 79–145.

Farrell, W. E., and J. A. Clark (1976), On postglacial sea-level, *Geophys. J. R. Astron. Soc.*, *46*, 647–667.

Gallagher, S. J., and G. Holdgate (2000), The palaeogeographic and palaeoenvironmental evolution of a Palaeogene mixed carbonate-siliciclastic cool-water succession in the Otway Basin, southeast Australia, *Palaeogeogr. Palaeoclimatol. Palaeoecol.*, *156*, 19–50.

Gallagher, S. J., K. Jonasson, and G. Holdgate (1999), Foraminiferal biofacies and palaeoenvironmental evolution of an Oligo-Miocene cool-water carbonate succession in the Otway Basin, southeast Australia, *J. Micropalaeontol.*, *18*, 143–168.

Gallagher, S. J., A. J. Smith, K. Jonasson, M. W. Wallace, G. R. Holdgate, J. Daniels, and D. Taylor (2001), The Miocene palaeoenvironmental and palaeoceanographic evolution of the Gippsland Basin, southeast Australia: A record of Southern Ocean change, *Palaeogeogr. Palaeoclimatol. Palaeoecol.*, *172*, 1–2.

Gallagher, S. J., D. R. Greenwood, D. Taylor, A. J. Smith, M. W. Wallace, and G. R. Holdgate (2003), The Pliocene climatic and environmental evolution of southeastern Australia: evidence from the marine and terrestrial realm, *Palaeogeogr. Palaeoclimatol. Palaeoecol.*, *193*, 349–382.

Gasson, E., M. Siddall, D. J. Lunt, O. J. L. Rackham, C. H. Lear, and D. Pollard (2012), Exploring uncertainties in the relationship between temperature, ice volume, and sea level over the past 50 million years, *Rev. Geophys.*, *50*, RG1005, doi:10.1029/2011RG000358.

Gornitz, V. (2009), Sea level change, post-glacial, in *Encyclopedia of Paleoclimatology and Ancient Environments*, edited by V. Gornitz, pp. 887–893, Springer, Dordrecht, Netherlands.

Gourley, T., and S. J. Gallagher (2004), Foraminiferal biofacies of the Miocene warm to cool climatic transition in the Port Phillip Basin, southeast Australia, *J. Foraminiferal Res.*, *34*, 294–307.

Gradstein, F. M., J. G. Ogg, and A. G. Smith, (2004), A Geologic Time Scale 2004, 589 pp., Cambridge Univ. Press, Cambridge, U. K.

Hegarty, K. A., I. R. Duddy, P. F. Green, A. J. W. Gleadow, I. Fraser, and J. K. Weissel (1986), Regional evaluation of the tectonic and thermal history of the Gippsland Basin, in Second South-Eastern Australia Oil Exploration Symposium, edited by R. C. Glenie, pp. 65–74, Pet. Explor. Soc. of Australia, Melbourne, Vict.

Heine, C., R. D. Muller, S. Bernhard, and L. DiCaprio (2010), Integrating deep Earth dynamics in paleogeographic reconstructions of Australia, *Tectonophysics*, *483*, 135–150.

Holdgate, G. R., and S. J. Gallagher (1997), Microfossil paleoenvironments and sequence stratigraphy of Tertiary cool-water carbonates, onshore Gippsland Basin, SE Australia, in Cool and Temperate Water Carbonates, vol. *56*, edited by N. P. James, and J. D. Clarke, pp. 205–220, Soc. for Sediment. Geol., Tulsa, Okla.

Huber, B. T., and F. Quillevere (2005), Revised Paleogene planktonic foraminiferal biozonation for the austral realm, *J. Foraminiferal Res.*, *35*, 299–314.

James, N. P., Y. Bone, L. B. Collins, and T. K. Kyser (2001), Surficial sediments of the Great Australian Bight: Facies dynamic and oceanography on a vast cool-water carbonate shelf, *J. Sedimen. Res.*, *71*, 549–567.

Katz, M. E., B. S. Cramer, J. R. Toggweiler, G. Esmay, C. Liu, K. G. Miller, Y. Rosenthal, B. S. Wade, and J. D. Wright (2011), Impact of Antarctic Circumpolar Current development on late Paleogene ocean structure, *Science*, *332*, 1076–1079.

Kominz, M. A., J. V. Browning, K. G. Miller, P. J. Sugarman, S. Mixintseva, and C. R. Scotese (2008), Late Cretaceous to miocene sea-level estimates from the new Jersey and Delaware coastal plain coreholes: An error analysis, *Basin Res.*, *20*, 211–226.

Li, L., S. J. Gallagher, and B. Finlayson (2000), Foraminiferal response to Holocene environmental changes of a tidal estuary in Victoria, southeastern Australia, *Mar. Micropaleontol.*, *39*, 229–246.

Li, Q., and B. McGowran (2000), Miocene foraminifera from Lakes Entrance oil shaft, Gippsland, southeastern Australia, *Mem. Assoc. Australasian Palaeontol.*, *22*, 142.

Li, Q., B. McGowran, N. P. James, and Y. Bone (1996a), Foraminiferal biofacies on the mid-latitude Lincoln Shelf, South Australia: Oceanographic and sedimentological implications, *Mar. Geol.*, *129*, 285–312.

Li, Q., B. McGowran, N. P. James, Y. Bone, and J. H. Cann (1996b), Mixed foraminiferal biofacies on the mesotrophic, mid-latitude Lacepede Shelf, South Australia, *Palaios*, *11*, 176–191.

Li, Q., P. J. Davies, B. McGowran, and T. van der Linden (2003), Foraminiferal ecostratigraphy of late Oligocene sequences, southeastern Australia: Patterns and inferred sea levels at third-order and Milankovitch scales, *Soc. Sediment. Geol. Spec. Publ.*, *75*, 147–171.

Martini, E. (1971), Standard Tertiary and Quaternary calcareous nannoplankton zonation, in Proceedings of the II Planktonic Conference, edited by A. Farinacci, pp. 739–777, Univ. of Calif., Berkeley, Calif.

McArthur, J. M., R. J. Howarth, and T. R. Bailey (2001), Strontium isotope stratigraphy: LOWESS version 3. Best-fit line to the marine Sr-isotope curve for 0 to 509 Ma and accompanying look-up table for deriving numerical age, *J. Geol.*, *109*, 155–169.

Miller, K. G., J. D. Wright, R. G. Fairbanks (1991), Unlocking the Ice House: Oligocene-Miocene oxygen isotopes, eustasy, and marine erosion, *J. Geophys. Res.*, *96*, 6829–6848.

Miller, K. G., M. A. Kominz, J. V. Browning, J. D. Wright, G. S. Mountain, M. E. Katz, P. J. Sugarman, B. S. Cramer, N. Christie-Blick, and S. F. Pekar (2005), The Phanerozoic record of global sea-level change, *Science*, *310*, 1293–1298.

Mitrovica, J. X., and G. A. Milne (2002), On the origin of late Holocene sea-level highstands within equatorial ocean basins, *Quat. Sci. Rev.*, *21*, 2179–2190.

Moucha, R., A. M. Forte, J. X. Mitrovica, D. B. Rowley, S. Quéré, N. A. Simmons, and S. P. Grand (2008), Dynamic topography and long-term sea-level variations: There is no such thing as a stable continental platform, *Earth Planet. Sci. Lett.*, *271*, 101–108.

Odin, G. S., and P. D. Fullagar (1988), Geological significance of the glaucony facies, *Dev. Sedimentol*, *45*, 295–332.

Okada, H., and D. Bukry (1980), Supplementary modification and introduction of code numbers to the low-latitude coccolith biostratigraphic zonation (Bukry, 1973; 1975), *Mar. Micropaleontol.*, *5*, 321–325.

Olaffson, G., and G. Villa (1992), Reliability of sphenoliths as zonal markers in Oligocene sediments from the Atlantic and Indian Oceans, *Mem. Sci. Geol.*, *43*, 261–275.

Pagani, M., J. C. Zachos, K. H. Freeman, B. Tipple, and S. Bohaty (2005), Marked decline in atmospheric carbon dioxide concentrations during the Paleogene, *Science*, *314*, 1894–1898.

Pälike, H., R. D. Norris, J. O. Herrle, P. A. Wilson, H. K. Coxall, C. H. Lear, N. J. Shackleton, A. K. Tripati, and B. S. Wade (2006), The heartbeat of the Oligocene climate system, *Science*, *314*, 1894–1898.

Pearson, P. N., G. L. Foster, and B. S. Wade (2009), Atmospheric carbon dioxide through the Eocene-Oligocene climate transition, *Nature*, *461*, 1110–1113.

Pekar, S. F., and N. Christie-Blick (2008), Resolving apparent conflicts between oceanographic and Antarctic climate records and evidence for a decrease in pCO (sub 2) during the Oligocene through early Miocene (34–16 Ma), *Palaeogeogr. Palaeoclimatol. Palaeoecol.*, *260*, 41–49.

Pekar, S. F., and K. G. Miller (1996), New Jersey Oligocene "Icehouse" sequences (ODP Leg 150X) correlated with global $\delta^{18}O$ and Exxon eustatic records, *Geology*, *24*, 567–570.

Pekar, S. F., N. Christie-Blick, M. A. Kominz, and K. G. Miller (2001), Evaluating the stratigraphic response to eustasy from Oligocene strata in New Jersey, *Geology*, *29*, 55–58.

Pekar, S. F., N. Christie-Blick, M. A. Kominz, and K. G. Miller (2002), Calibration between eustatic estimates from backstripping and oxygen isotopic records for the Oligocene, *Geology*, *30*, 903–906.

Pekar, S. F., R. M. De Conto, and D. M. Harwood (2006), Resolving a late oligocene conundrum: Deep-sea warming and Antarctic glaciation, *Palaeogeogr. Palaeoclimatol. Palaeoecol.*, *231*, 29–40.

Pettijohn, E. J. (1975), Sedimentary Rocks, 3rd ed., 628 pp., Harper and Row, New York.

Pollard, D., and R. M. DeConto (2005), Hysteresis in Cenozoic Antarctic ice-sheet variations, *Global Planet. Change*, *45*, 9–12.

Rahmanian, V. D., P. S. Moore, W. J. Mudge, and D. E. Spring (1990), Sequence stratigraphy and the habitat of hydrocarbons, gippsland Basin, Australia, in Classic Petroleum Provinces, edited by J. Brooks, pp. 525–541, Geol. Soc., London, U. K.

Shackleton, N. J., and M. A. Hall (1990), Carbon isotope stratigraphy of bulk sediments, ODP Sites 689 and 690, Maud Rise, Antactica, *Proc. Ocean Drilling Prog. Sci. Results*, *113*, 985–989.

Smith, A. J. (2002), The recent foraminiferal ecology of southeastern Australia and its use in palaeoenvironmental interpretation, Ph.D. thesis, Univ. of Melbourne, Melbourne, Vict.

Smith, A. J., and S. J. Gallagher (2003), The recent foraminifera and facies of the Bass Canyon: A temperate submarine canyon in Gippsland, Australia, *J. Micropalaeontol.*, *22*, 63–83.

Smith, A. J., S. J. Gallagher, M. W. Wallace, G. R. Holdgate, J. Daniels, and J. Keene (2001), The recent temperate foraminiferal biofacies of the Gippsland Shelf: An analogue for Neogene environmental analyses in southeastern Australia, *J. Micropalaeontol.*, *20*, 127–142.

Solomon, S., et al. (2007), Intergovernmental Panel on Climate Change, The Physical Science Basis: Contribution of Working Group 1 to the Fourth Assessment Report of the Intergovernmental Panel on Climate Change, Cambridge Univ. Press, Cambridge, U. K.

Spezzaferri, S., I. Premoli Silva, and A. Boersma (1991), Oligocene planktonic foraminiferal biostratigraphy and paleoclimatic interpretation from Hole 538A, DSDP Leg 77, Gulf of Mexico, *Palaeogeogr. Palaeoclimatol. Palaeoecol.*, *83*, 217–263.

Stickley, C. E., H. Brinkhuis, S. A. Schellenberg, A. Sluijs, U. Röhl, M. Fuller, M. Grauert, M. Huber, J. Warnaar, and G. L. Williams (2004), Timing and nature of the deepening of the Tasmanian Gateway, *Paleoceanography*, *19*, PA4027, doi:10.1029/2004PA001022.

Swart, P. K. (2008), Global synchronous changes in carbon isotopic composition of carbonate sediments unrelated to changes in global carbon cycle, *Proc. Natl. Acad. Sci.*, *105*, 13,741–13,745.

van der Zwann, G. J., F. J. Jorissen, and H. C. De Stigter (1990), The depth dependency of planktonic/benthonic foraminiferal ratios, *Mar. Geol.*, *95*, 1–16.

van Hinsbergen, D. J. J., T. J. Kouwenhoven, and G. J. van der Zwaan (2005), Paleobathymetry in the backstripping procedure: Correction for oxygenation effects on depth estimates, *Palaeogeogr. Palaeoclimatol. Palaeoecol.*, *221*, 245–265.

Villa, G., C. Fioroni, L. Pea, S. Bohaty, and D. Persico (2008), Middle Eocene-late Oligocene climate variability: Calcareous nannofossil response at Kerguelen Plateau, Site 748, *Mar. Micropaleontol.*, *69*, 173–192.

Wade, B. S. and H. Pälike (2004), Oligocene climate dynamics, *Paleoceanography*, *19*, PA4019, doi:10.1029/2004PA001042.

Wade, B. S., W. A. Berggren, and R. K. Olsson (2007), The biostratigraphy and paleobiology of Oligocene planktonic Foraminifera from the equatorial Pacific Ocean (ODP Site 1218), *Mar. Micropaleontol.*, *62*, 167–179.

Wade, B.S., P. N. Pearson, W. A. Berggren, and H. Pälike (2011), Review and revision of Cenozoic tropical planktonic foraminiferal biostratigraphy and calibration to the geomagnetic polarity and astronomical time scale, *Earth Sci. Rev.*, *104*, 111–142.

Walcott, R. I. (1972), Past sea levels, eustasy and deformation of the Earth, *Quat. Res.*, *2*, 1–14.

Wallace, M. W., G. R. Holdgate, J. Daniels, S. J. Gallagher, and A. Smith (2002), Sonic velocity, submarine canyons, and burial diagenesis in Oligocene-Holocene cool-water carbonates, Gippsland Basin southeast Australia, *AAPG Bull.*, *86*, 1593–1607.

Watts, A. B., (2001), Isostasy and Flexure of the Lithosphere, 458 pp., Cambridge Univ. Press, Cambridge, U. K.

Westphal, H., F. Hilgen, and A. Munnecke (2010), An assessment of the suitability of individual rhythmic carbonate successions for astrochronological application, *Earth Sci. Rev.*, *99*, 19–30.

Zachos, J., M. Pagani, L. Sloan, E. Thomas, and K. Billups (2001), Trends, rhythms, and aberrations in global climate 65 Ma to present, *Science*, *292*, 686–693.

Zachos, J., G. R. Dickens, and R. E. Zeebe (2008), An early Cenozoic perspective on greenhouse warming and carbon-cycle dynamics, *Nature*, *451*, 279–283.